Journal of Materials Chemistry A

Accepted Manuscript

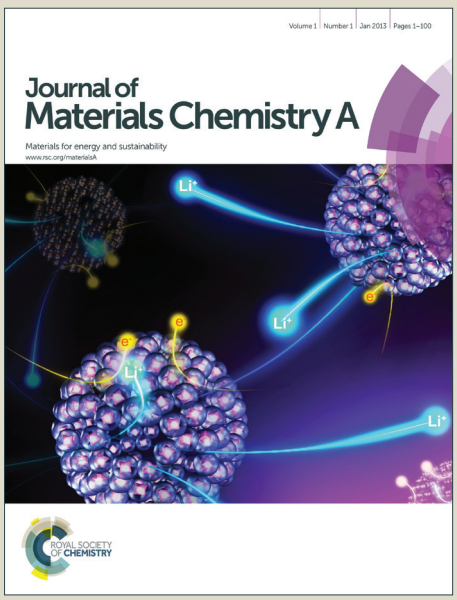

ROYAL SOCIETY OF CHEMISTRY

www.rsc.org/materialsA

Diethylenetriamine (DETA) - Assisted Anchoring of Co_3O_4 Nanorods on Carbon Nanotubes as Efficient Electrocatalyst for Oxygen Evolution Reaction

Yu-Xia Zhang, Xin Guo, Xue Zhai, Yi-Ming Yan,** and Ke-Ning Sun *

Beijing Key Laboratory for Chemical Power Source and Green Catalysis, School of Chemical Engineering and Environment, Beijing Institute of Technology, Beijing, 100081,People's Republic of China.

Corresponding Authors.

Fax: +86-10-68918696;

[*] E-mail: bitkeningsun@163.com

[**]E-mail: bityanyiming@163.com ;

Abstract

Co_3O_4 nanorods-multiwalled carbon nanotubes hybrid (Co_3O_4@MWCNT) has been fabricated as a highly efficient electrocatalyst for water oxidation in alkaline electrolyte. The well-defined Co_3O_4 nanorods were successfully anchored onto mildly oxidized MWCNTs with the assistance of diethylenetriamine (DETA) following a simple route. The as-prepared hybrid possesses promising BET specific surface areas about 252 m^2 g^{-1} and shows excellent electrocatalytic activity towards oxygen evolution reactions (OER) with an onset potential of about 0.47 V *vs.* Ag/AgCl and an overpotential of 309 mV to achieve a current density of 10 mA cm^{-2} in 1.0 mol L^{-1} KOH. In addition, the Co_3O_4@MWCNT catalyst exhibits prominent stability during long-term electrolysis of water. We attribute the enhanced performance to a synergic effect between MWCNT and Co_3O_4 nanorods by gaining insight into the electrochemical properties of the Co_3O_4@MWCNT hybrid. This work offers a useful way to synthesis 1D metal oxides combined with 1D carbon materials for wide applications in energy storage and conversion.

Keywords: Co_3O_4, nanorods, DETA, multi-walled carbon nanotubes, oxygen evolution reaction

1. Introduction

Electrochemical water splitting that produces hydrogen and oxygen is an environmentally benign method to store electricity generated from renewable energy sources such as solar and wind [1–6]. However, the efficiency of electrochemical water splitting is usually low due to high overpotentials and low currents associated with the oxygen-evolving reaction (OER).[7,8] To expedite the kinetic of OER, efficient electrocatalysts, such as Pt, RuO_2, [9] and IrO_2 ,[10] have been widely used as commercial products. Despite the fact that RuO_2 and IrO_2 exhibit low OER overpotentials and high current densities, they suffer from high cost and poor long-term stability in alkaline media, therefore limiting the practical applications.[11]

Recently, novel OER electrocatalysts based on inexpensive and abundant materials such as manganese (Mn),[12] nickel (Ni) ,[13] and cobalt (Co) [14–16] have been intensively investigated because that their electrocatalytical activities towards OER are comparable to that of noble metal-based electrocatalysts. Among these OER electrocatalysts, spinel cobaltite oxides (such as Co_3O_4) have attracted considerable attentions as effective anode materials for oxygen evolution in alkaline solution. [17-19] However, Co-based catalysts, such as Co_3O_4, have shown disadvantages including strong causticity in alkaline solution, intrinsic poor electrical conductivity, and undesirable morphology or crystalline structure.[18] To circumvent these problems, it is favorable to utilize a suitable substrate to support the Co-based catalysts in a rational manner, therefore achieving an enhanced electrocatalytical performance. The required substrates should be preferably conductive, high specific surface area, and mechanical stability in order to stabilize the uniformly dispersed electrocatalyst at the surface and maximize the electrocatalytic activity. As a member of carbon-based nanomaterials, carbon nanotube (CNT) has unique properties such as high electrical conductivity, large surface area, high mechanical strength, and structural flexibility, therefore offering an ideal scaffold for supporting Co-based electrcatalysts. [18-23] Indeed, CNT supported Co-based electro-catalysts have already been used for OER with improved catalytic activity and stability. For instance, Xie et.al. [18] reported the Co_3O_4 nanocrystals on single-walled carbon nanotubes as OER catalysts, focusing on the enhanced durability of the resulted hybrid in neutral conditions. Zhao et. al. [19] demonstrated that mildly oxidized multi-walled carbon nanotubes (MWCNTs) can be used to combine Co_3O_4 nanoparticle with oxygen-containing groups, while the inner-wall of MWCNTs acts as highly conducting network.

On the other hand, it is known that the properties of the metal oxides strongly depend on their morphologies and structures, such as crystal sizes, orientations, stacking manners, aspect ratios and even crystalline densities.[24-29] Thus, rational design of morphology and structure of Co_3O_4 is an effective route to afford high activity for Co_3O_4 in electrochemical applications. In general, nanorod-shaped materials have high surface-to-volume ratio [36] and mainly exposes (110) crystal planes, which is considered as highly activated facet for CO oxidation, methane combustion and ethylene oxidation [25-28], (110) crystal planes with high energies should reduce the oxidation–reduction gaps, thereby considerably accelerate the reaction rates. As such, we expect that Co_3O_4 nanorods anchoring on CNTs should generate a novel composite with promising OER performance. So far, only

nanoparticles [18,19, 30-32] or other irregular structured [33-35] Co_3O_4 in Co_3O_4-CNT composites have been reported. Therefore, it is scientific significant to realize the anchoring of 1-D Co_3O_4 nanorod on 1-D CNT towards electrochemical water oxidation, while the technique challenge is remaining.

Herein, we report the synthesis of nanorod-shaped Co_3O_4 anchored on MWCNTs with the assistance of diethylenetriamine (DETA) to obtain a novel electrocatalyst with high OER efficiency. The hybrid is prepared by a mild solution-phase synthesis step. The DETA is chosen because that it acts as dispersing agent, as well as helps to produce nanorod-shaped Co_3O_4 and favors the growth of Co_3O_4 nanorods on MWCNTs. We demonstrate that the resulting Co_3O_4@MWCNT hybrid shows excellent OER performance and good stability in alkaline solutions due to its fast electron transport properties and highly exposed activated crystal planes of {110}.

2. Experimental section

2.1 Chemicals: $Co(Ac)_2 \cdot 4H_2O$ (97%, Nacalai tesque), Multiple walled carbon nanotubes (MWCNTs, OD: 20-30 nm, length: 1-2 μm , Beijing Nachen S&T Ltd) , sodium carbonate (99.5%, Merck), ethylene glycol ($C_2H_6O_2$, absolute for analysis, ACS, Merck) , diethylenetriamine (DETA; 99%, Sigma-Aldrich) were used as received without further purification.

2.2 Purification and oxidation of MWCNTs: In a typical procedure, 850 mg MWCNTs were initially mixed with concentrated hydrogen nitrate (HNO_3) (200 mL, 4 mol L^{-1}) and ultrasonicated for 1.0 h, followed by water bath at 80 °C under magnetic stirring for 3.0 h to remove metallic and organic impurities and obtain oxygen-containing groups. Then, the resulting mixture was washed with deionized water several times until pH was = 7.0, and next the mildly oxidized MWCNTs were dried at 60 °C.

2.3 Preparation of the Co_3O_4@MWCNT, Co_3O_4-MWCNT, Co_3O_4 composites: Typically, 50 mg acid-treated MWCNTs were dispersed in 18.5 mL of ethylene glycol by sonication for 20 minutes, then the mixture was transferred to a three-necked bottle (capacity of 250 mL) and put in a flask heating mantle with refluxing, and then nitrogen flow was introduced at a constant rate, followed by addition of 1.5 g $Co(Ac)_2 \cdot 4H_2O$ and 30 μL diethylenetriamine (DETA; 99%, Sigma-Aldrich) under magnetic stirring. After stirring for 2 minutes, the system was heated up until the temperature rose to 160 °C. Then, 60 mL of 0.2 M sodium carbonate aqueous solution was added to the solution drop by drop. The precipitate was further aged for 8.5 h and then was centrifuged followed by thoroughly washing with distilled water and ethanol for several times, and then vacuum-drying at 55 °C overnight. Finally, the resulting product was heat-treated at 350 °C for 4.0 hour in Ar atmosphere. For a control experiment, Co_3O_4-MWCNT was prepared following the same steps as Co_3O_4@MWCNT without adding DETA. Also, Co_3O_4

nanorods were made in the same steps as Co_3O_4@MWCNT without adding MWCNTs and DETA, referring to a reported process with some modifications.[37]

2.4 Characterizations: The morphology was characterized by the scanning electron microscope (SEM, QUANTA FEG 250) and transmission electron microscope (TEM, FEI Tecnai G2 F30 S-TWIN). The obtained products were characterized by X-ray diffraction (XRD, Rigaku Ultima IV, Cu Kα radiation, 40 KV, 40 mA). Raman spectra was performed on a RM 2000 microscopic confocal Raman spectrometer (Renishaw in via Plus, England) employing a 514 nm laser beam. X-ray photoelectron spectroscopy (XPS) was carried out on Physical Electronics 5400 ESCA. Raman was performed on Renishaw RM 2000 with 633 nm laser. Inductively Coupled Plasma-Atomic Emission Spectrometry (ICP-AES) was carried on Profile Spec to determine the content of cobalt element. Brunauer−Emmett−Teller (BET) measurements using N_2 absorption was performed on Autosorb-IQ2-MP-C system.

2.5 Electrochemical Measurements: 1.0 mg of catalyst was dispersed in a mixture of 850 μL alcohol and 15 μL Nafion solution and sonicated to form homogeneous ink. Then, 10 μL of the dispersion was drop-dried onto the surface of glass carbon rotating disk electrode (RDE, PINE, 5.61 mm diameter), leading to the catalyst loading ~0.05 mg cm^{-2}, disk area: 0.25 cm^2. The as-prepared catalyst decorated RDE working electrode, a Pt wire counter electrode, and an Ag/AgCl (3 M KCl) reference electrode constituted a three-electrode electrochemical cell, which was conducted with a CHI 760 Electrochemical Workstation. Electrochemical tests were performed at room temperature.

Linear sweep voltammetry was obtained by sweeping the potential from 0.3 to 1.2 V *vs*. Ag/AgCl at room temperature with a sweep rate of 1.0 mV s^{-1}, and the j (mA cm^2) in this work is normalized by geometric area of the glassy carbon electrode (0.25 cm^2), marked as j_{geo}. Experiments involving RDE were carried out with the working electrode continuously rotating at 2000 rpm to get rid of the oxygen bubbles. The catalyst was applied for a number of potential sweeps until the data was stable before polarization curves were measured, which were all corrected with 95% IR-compensation.

3. Results and discussion

3.1. Characterization of Co_3O_4 and Co_3O_4@MWCNT.

The degree of oxidation for MWCNT is very important for the follow-up synthesis process. The functional groups on the outer-walls of CNTs help to nucleate and anchor nano-sized electrocatalyst, while the highly electrical conductive inner-walls of CNTs are very important networks for electron transport. Here, we chose the mildly oxidized MWCNTs as substrate which contains functional groups on outer walls and maintains inside wall as conducting access. Scheme 1 shows the synthesis process

of Co_3O_4@MWCNT hybrid. Firstly, the amino group of DETA can effectively interact with MWCNTs via physisorption or electrostatic adsorption. Subsequently, the Co^{2+} cations were introduced to DETA through a specific interaction and an inductive effect.[38] Meanwhile, it is known that polar weak capping agent, which tends to adsorb on {110}. [29] Thus, polar DETA should tend to adsorb on {110}, thus contributing to the growth of nanorod. Subsequently, with the addition of sodium carbonate, cobalt hydroxide acetate was produced following a gradually intercalation of carbonate anions into the interlayers.[37] The Co_3O_4@MWCNT was finally observed by aging the formed cobalt hydroxide acetate at 160 °C, and then calcination for 4 hour.

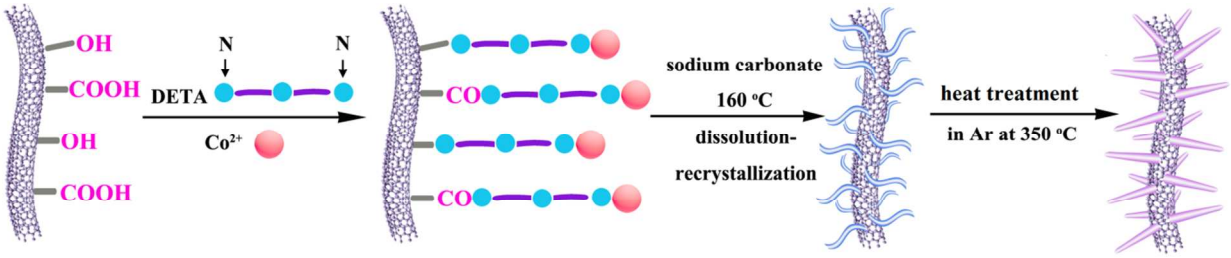

Scheme 1. Schematic illustration of the preparation process of Co_3O_4@MWCNT hybrid

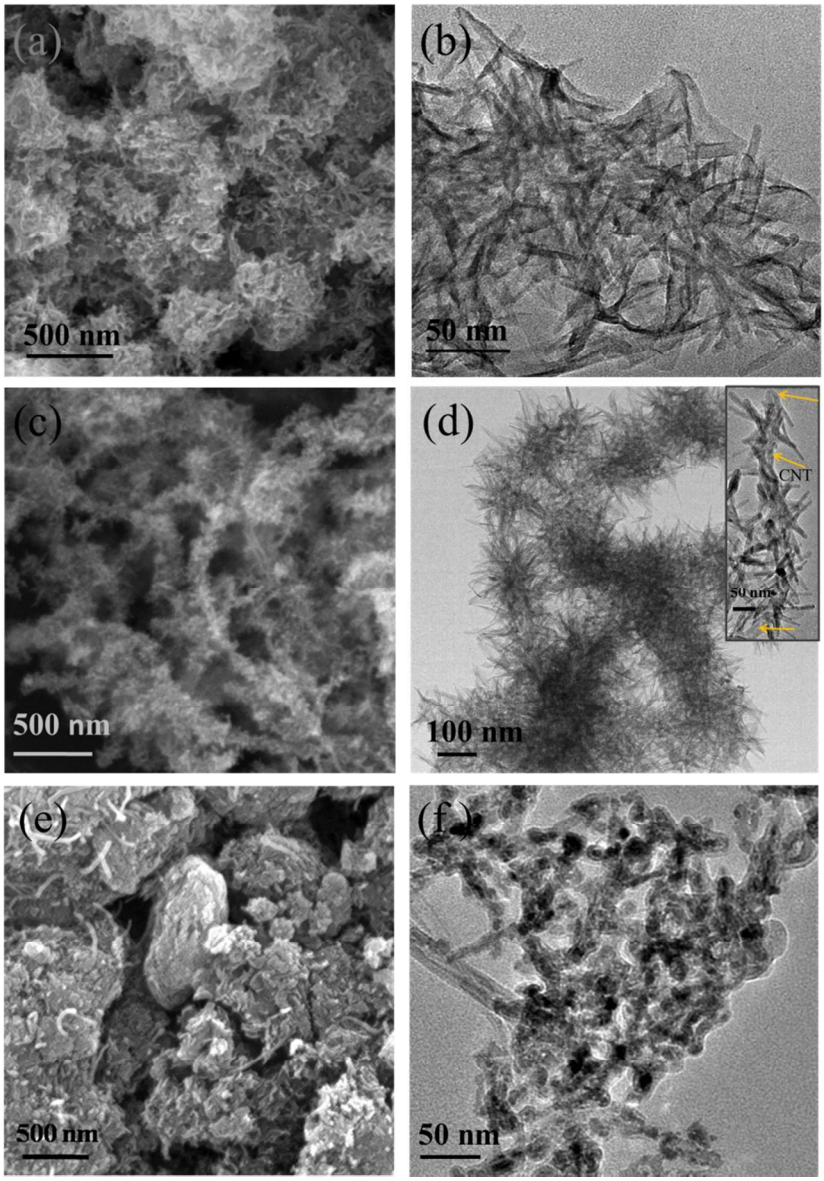

Figure 1. (a) SEM image of Co_3O_4. (b) TEM image of Co_3O_4. (c) SEM image of Co_3O_4@MWCNT. (d) TEM images of Co_3O_4@MWCNT. (e) SEM image of Co_3O_4-MWCNT. (f) TEM image of Co_3O_4-MWCNT

Figure 1 presents the SEM and TEM images of the synthesized Co_3O_4, Co_3O_4-MWCNT and Co_3O_4@MWCNT, displaying the morphology and microstructure of the samples. As shown, pure Co_3O_4 sample showed nanocrystalized structure with a diameter of about 10 nm and a length of 100-200 nm, (Figure 1a, b) which was similar to the results reported previously. [37] In comparison, the Co_3O_4@MWCNT sample showed a clearly different morphology, as shown in Figure 1c, d, the Co_3O_4 units were kept well-defined nanorods shape, closely wrapped on the nanotubes, resulting a unique 1D plus 1D structure. However, the sample of Co_3O_4-MWCNT, which was synthesized without the addition of DETA, displayed irregular particles mixed with tangled

MWCNTs (Figure 1e, f). Moreover, it can be seen the Co_3O_4 nanoparticles tended to aggregated and MWCNT were not fully covered, which demonstrates that the DETA plays important role in synthesizing particular shaped-Co_3O_4@MWCNT, as shown in Scheme 1. The TEM images of Co_3O_4-MWCNT and Co_3O_4@MWCNT firmly demonstrated the crucial role of DETA on the structure of the resulted catalysts. The apparent difference in the morphology of the Co_3O_4@MWCNT and Co_3O_4-MWCNT should be explained by the fact that DETA either help to disperse the MWCNTs in the solution, or contribute to the growth of Co_3O_4 nanorods on the MWCNTs. Figure S1 shows the SEM image of the Co_3O_4- MWCNT hybrid synthesized with raw MWCNT. Obviously, it displays a simple mixture of MWCNT with thin Co_3O_4 particles. It seems that DETA could physically adsorb onto MWCNT. However, a close comparison of the SEM results shows very different morphology for the catalysts prepared with raw MWCNT and mildly oxidized MWCNT (Figure S1 and Figure 1c). The regular structure and well-defined morphology of Co_3O_4@MWCNT strongly demonstrate that oxidized MWCNT should benefit from electrostatic interactions between oxygen containing groups on the oxidized MWCNT and DETA, therefore contributing to the uniform growth of Co_3O_4 on MWCNT.

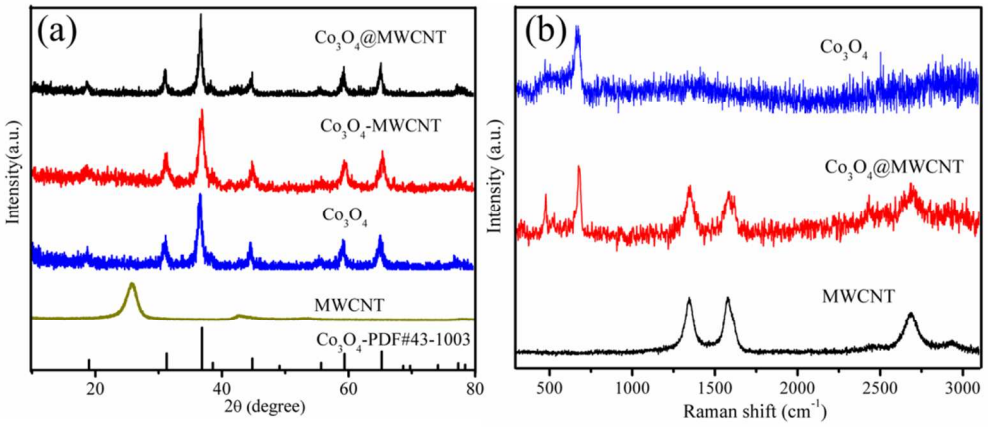

Figure 2. (a) XRD pattern of Co_3O_4 and Co_3O_4@MWCNT hybrid. (b) Raman spectra of the Co_3O_4 and Co_3O_4@MWCNT hybrid.

In order to further identify chemical composition and structure of the prepared samples, powder X-ray diffraction (XRD) characterization was conducted. As shown in Figure 2a, the XRD spectrums of the three samples showed the existence of spinel crystalline structured Co_3O_4 (PDF: 43-1003). We noted that the XRD spectrum of Co_3O_4, Co_3O_4-MWCNT and Co_3O_4@MWCNT hybrid were nearly the same, while the 2θ values of 26° and 43°, assigning to the diffraction peak of MWCNTs, were not clearly observed at Co_3O_4-MWCNT and Co_3O_4@MWCNT samples. This phenomenon should be either probably due to a low content of CNTs in the hybrid, or possibly attributed to the blocking effect from the strong peaks of Co_3O_4. As for Co_3O_4-MWCNT, Figure 1e clearly shows the existence of MWCNTs. To further demonstrate the existence of MWCNTs in the Co_3O_4@MWCNT hybrid, X-ray photoelectron spectroscopy (XPS) and Raman spectroscopy were given in Figure S2 and

Figure 2b, respectively. XPS spectra of Co_3O_4@MWCNT (Figure S2) display intense, Co 2p peaks with binding energies of about 781 eV are characteristic of Co_3O_4 species, while C 1s peaks with binding energies of about 284 eV indicate the presence of carbon from MWCNT. As shown in the inset enlarged figure around 780 eV, the XPS peak assigned to Co 2p of pure Co_3O_4 in the region around 780.2 eV, the shift of the peak for Co 2p of the Co_3O_4@MWCNT hybrid at 781.5 eV and for Co_3O_4-MWCNT at 781.1 eV can probably be attributed to the interactions between Co_3O_4 and MWCNT. These different BE shifting data in XPS spectra for the three samples confirm the successful assembly of Co_3O_4 nanorods on MWCNT.[18] As shown in Figure 2b, the Raman spectrum of Co_3O_4 exhibited three well-defined Raman peaks at 477.1, 507.8 and 671.1 cm^{-1}, which were assigned to the Raman active modes of Co_3O_4 (i.e., T_{2g}, E_g, and A_{1g} symmetries) [39-41], while MWCNT exhibited three strong peaks at 1345.2, 1580.8 and 2687.6 cm^{-1}, respectively. For the Raman spectra of Co_3O_4@MWCNT hybrid, the peaks at 478, 515.5 and 673.6, assigning to Co_3O_4, and the peaks at 1341.8, 1580.8 and 2683.0, corresponding to MWCNTs were clearly observed. We next performed TGA test to estimate the mass content of MWCNTs in Co_3O_4@MWCNT, which the value is ca. 34%.

3.2. Electrochemical Properties of Co_3O_4 and Co_3O_4@MWCNT.

To assess the OER catalytic activity of Co_3O_4@MWCNT, the sample was investigated by a series of electrochemical experiments. The ohmic potential drop (iR) losses that arise from the solution resistance were all corrected (Figure S3). Linear sweep voltagrams (LSVs) showed that the OER onset potential of Co_3O_4@MWCNT hybrid was about 474 mV (vs. Ag/AgCl) in 1 M KOH (an overpotential only about 268 mV, $E°_{H2O/O2}$ = 205.6 mV vs. Ag/AgCl at pH 14), which was much more positive than that of the Co_3O_4-MWCNT and pure Co_3O_4 electrodes, as shown in Figure 3a. Specifically, current response of Co_3O_4 nanorods modified electrodes was lower than that of Co_3O_4@MWCNT electrode. Also, the onset potential of Co_3O_4 electrode was ~503 mV, which was about 30 mV higher than that of Co_3O_4@MWCNT. As the control experiments, the MWCNTs electrode and blank RDE electrode showed negligible current response toward OER. Meanwhile, to achieve a current density j_{geo} = 10 mA cm^{-2}, an applied potential of E_{app}= 515 mV (vs. Ag/AgCl) was required, corresponding to small overpotential of *ca.* 310 mV. The excellent performance is comparable to that of reported IrO_x and Co_3O_4 nanoparticle as OER catalysts in alkaline media.[14,19,24] Similar LSVs measurements were further performed in 0.1 M KOH solution (as shown in Figure S4). Again, the Co_3O_4@MWCNT electrode exhibited the best OER catalytic activities among all the electrodes. The results strongly demonstrate that the Co_3O_4@MWCNT hybrid has excellent OER catalytic activities in alkaline solution in comparison to pure Co_3O_4 or MWCNT, which was probably contributed from a synergistic effect between Co_3O_4 and MWCNTs components in the Co_3O_4@MWCNT hybrid.

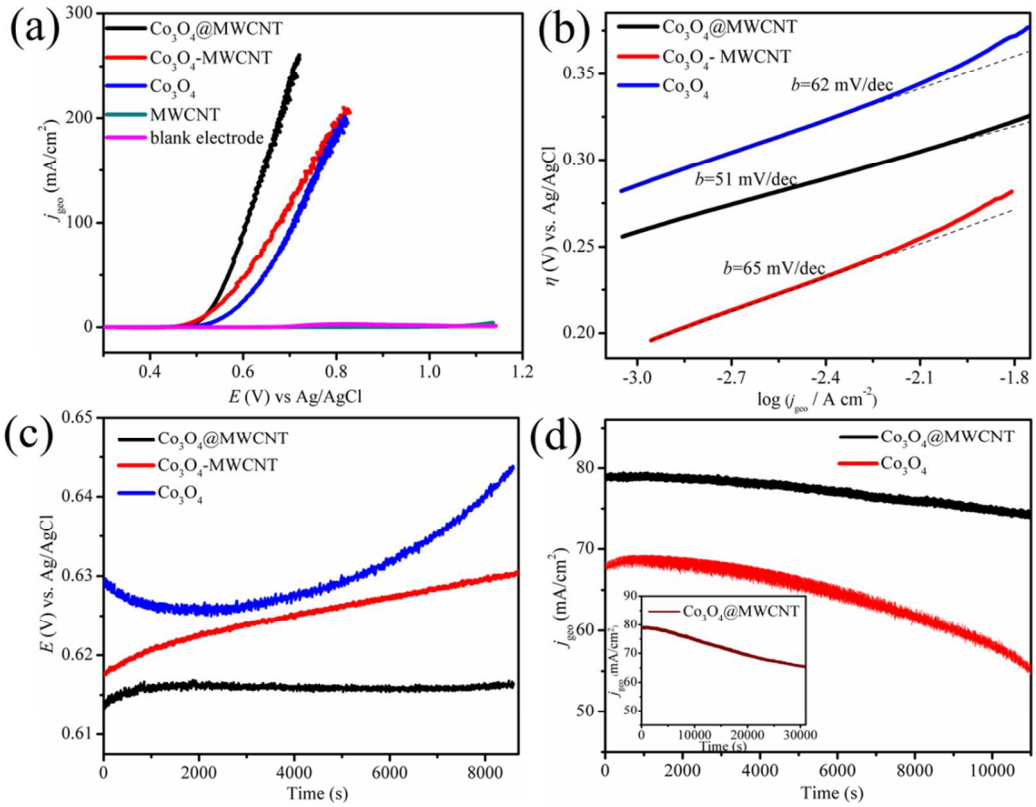

Figure 3. (a) Linear sweep voltammetry curves (LSVs) obtained with RDE modified with Co_3O_4@MWCNT, Co_3O_4-MWCNT hybrid, Co_3O_4, MWCNTs and nothing, respectively, at 1 mV s^{-1} (after iR compensation). (b) Tafel plot of Co_3O_4@MWCNT, Co_3O_4-MWCNT and Co_3O_4 derived from (a) (overpotential $\eta = E_{app} - E°_{H2O/O2}$). Scan rate=1 mV s^{-1}. (c) Galvanostatic OER profiles at j = 20 mA cm^{-2} of Co_3O_4@MWCNT composite and Co_3O_4 in 1 M KOH. (d) Current profiles during 11000 s electrolysis at 0.8 V using Co_3O_4@MWCNT composite and Co_3O_4. Experimental conditions: 1 M KOH, T=298 K, glassy carbon electrodes of RDE at 2000 rpm.

To further demonstrate the advantage of the Co_3O_4@MWCNT hybrid, it is tempting to probe the OER kinetics using Tafel plots, as shown in Figure 3b. All the Tafel plots for Co_3O_4@MWCNT, Co_3O_4-MWCNT and Co_3O_4 electrode displayed a linear dependence of the logarithm of current density in 1.0 M KOH. We found that the Tafel slope for pure Co_3O_4 and Co_3O_4-MWCNT were 62 mV and 65 mV per decade, respectively, while the Co_3O_4@MWCNT afforded smaller Tafel slope down to 51 mV dec^{-1}. The observed decrease in the Tafel slope values might be caused by a synergistic coupling effect between Co_3O_4 and MWCNT. Moreover, in the absence of DETA, the Co_3O_4-MWCNT shows irregular Co_3O_4 particles mixed with tangled MWCNTs, and this insufficient contact between Co_3O_4 and MWCNT might weaken the synergistic coupling between Co_3O_4 and MWCNT in Co_3O_4-MWCNT than that of Co_3O_4@MWCNT, leading to weaker kinetic of Co_3O_4-MWCNT. We noted that DETA didn't introduce "N" functionalities in such hybrid assemblies, which can be proved by the inset of Figure S2. The using of

DETA is mainly help to tightly and uniformly anchor Co_3O_4 nanorods on MWCNTs, therefore enhancing the synergistic coupling between Co_3O_4 and MWCNT.

The stability test for Co_3O_4@MWCNT composite was carried out by continuously performing the OER on modified RDE under alkaline conditions. Galvanostatic curves for Co_3O_4@MWCNT, Co_3O_4-MWCNT and Co_3O_4 were recorded for over 9000 s, as shown in Figure 3c. Only slight change of the potential for Co_3O_4@MWCNT was observed, while apparent deviation of the potential for Co_3O_4-MWCNT and Co_3O_4 was found, suggesting better alkaline tolerance of Co_3O_4@MWCNT than that of Co_3O_4-MWCNT and Co_3O_4. Moreover, the potential change of Co_3O_4-MWCNT is less than that of Co_3O_4@MWCN, illustrating that the addition of DETA not only helps the successful synthesis of Co_3O_4@MWCNT, but further improves the stability of Co_3O_4@MWCNT. To further demonstrate the stability of the Co_3O_4@MWCNT catalyst, electrolysis of water was carried out over 11000 s in 1 M KOH aqueous solution at 0.8 V *vs.* Ag/AgCl, as shown in Figure 3d. As seen, the catalytic current density of Co_3O_4@MWCNT decreased from 79 mA cm^{-2} to 74 mA cm^{-2}, the degrading value is about 6.3 % of the initial value, which was probably caused by partial desorption of the catalyst from the RDE or the degradation of the electrolytes (e.g. pH and conductivity change), the inset of Figure 3d shows the value of j_{geo} decreased about 15.4% during 30000 s (from 79 mA cm^{-2} to 66 mA cm^{-2}). In comparison, the catalytic current density of Co_3O_4 showed the decay from 68 mA cm^{-2} to 55 mA cm^{-2} during 11000 s, the degrading value is about 19.1 % of the initial value. Furthermore, the j_{geo} of Co_3O_4 is always lower than that of Co_3O_4@MWCNT, clearly indicating much poorer stability of the Co_3O_4 sample. We assumed that the presence of MWCNTs in the Co_3O_4@MWCNT should help to improve the stability by preventing the strong causticity from the alkaline electrolyte.

Per-metal turnover frequency (TOF) is an important parameter in assessing the OER performance of the catalysts. Based on the obtained data, the TOF can be calculated by measuring the current density for the $4e^-/4H^+$ OER process on Co_3O_4@MWCNT electrode. Moreover, inductively coupled plasma emission spectrometer (ICP) results showed the mass content of Co is ca. 7.786 mmol g^{-1}. As a result, the TOF of Co_3O_4@MWCNT was calculated and compared with the results obtained with other cobalt-based catalysts. (Table S1) We noted that the TOF was estimated by assuming that every Co atom is involved in the catalysis.

We further carried out gas chromatography to identify the product at the Co_3O_4@MWCNT anode chamber (Figure S5). It shows that, along with the continuous electrolysis at 0.8 V at Co_3O_4@MWCNT anode, the produced O_2 was increased, correspondingly. Moreover, we noted that there is no CO or CO_2, the possible oxidation products of CNTs, can be detected during the course of 2 h electrolysis of water at 0.6 V (ca.10 mA cm^{-2}). The above results clearly demonstrate that Co_3O_4@MWCNT, which was synthesized with the assistance of DETA, are excellent OER catalyst in terms of catalytical activity and stability, comparing to Co_3O_4 nanorods and MWCNTs. We believed that the mild oxidized MWCNTs, allowing for the balance of the surface oxidation and structural integrity of the CNTs, can act as suitable substrate for anchoring Co_3O_4

nanorods, thus attaining high OER activity. We attribute the enhanced OER performance for Co_3O_4@MWCNT to the following possible reasons.

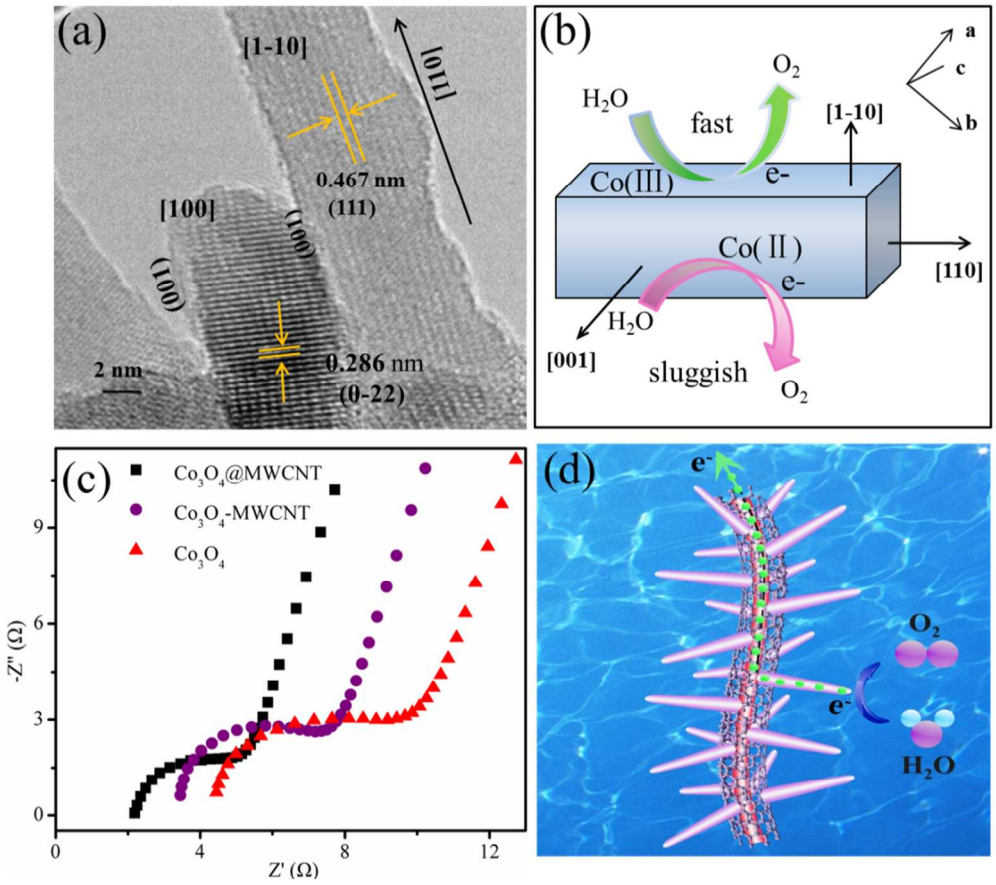

Figure 4. (a) The HRTEM images of Co_3O_4 nanorod of Co_3O_4@MWCNT. (b) Schematic illustration of the water oxidation on nanorod surface and the nanorod morphology highlighting the exposed surfaces. Note: [uvw] is an index of a specified crystal axis, and (hkl) is an index of specified crystal plane. (c) Complex impedance plot for the Co_3O_4@MWCNT hybrid and Co_3O_4 at 0.6 V *vs* Ag/AgCl. Experimental conditions: T = 298 K, 1 M KOH solution; work electrode: glassy carbon electrodes of RDE modified by Co_3O_4@MWCNT and Co_3O_4. (d) Schematic illustration of the water oxidation under the synergetic effect under the Co_3O_4 nanorod and MWCNT of hybrid.

1) The observed promising activity should arise from the unique structure and morphology of the Co_3O_4@MWCNT hybrid. We have mentioned that nanorods-shaped Co_3O_4 is favorable for OER due to the special crystalline properties. To verify this, high resolution TEM (HRTEM) was used to characterize the morphological and structural properties. Figure 4a shows the crystallographic of the Co_3O_4 nanorod anchored in MWCNTs, displaying a section of Co_3O_4 nanorod in the [1-10] orientation. It revealed that the naonorods was grown along the [110] direction, which was constructed from {111} planes, with a flat side parallel to [001]. In the [100] orientation, which was constructed from {022} planes with a spacing of 0.286 nm, these (001) side planes were also observed. Taking into account of the HRTEM results, a carton illustration was presented to show the crystalline structure of the anchored Co_3O_4 nanorods on MWCNTs, as shown in Figure 4b. Therefore, the preferentially exposed crystal

planes for the Co_3O_4 nanorods in Co_3O_4@MWCNT hybrid, including two side planes and two end planes, can be determined to be {110}. It is known that the {110} planes are composed mainly of Co^{3+} cations, which are regarded as the most active sites for ethylene oxidation [42] and CO oxidation[43]. Therefore, it is reasonable to postulate that predominant {110} planes that are composed of rich Co^{3+} species in the Co_3O_4 nanorods could result in high OER activity.

2) Brunauer–Emmett–Teller (BET) measurements show that the BET specific surface areas of Co_3O_4@MWCNT, Co_3O_4-MWCNT and Co_3O_4 are about 252.5 m^2 g^{-1}, 219.8 m^2 g^{-1} and 218.4 m^2 g^{-1}, respectively. It suggests that the incorporation of MWCNT helps to increase the surface areas of the resulted hybrid. The impressively large surface area of Co_3O_4@MWCNT offers a high density of Co^{3+} active sites available for surface reactions [36].

3) MWCNTs are relatively chemically inert and have been reported to be stable under strong oxidative environments. The result from gas chromatography has evident that no possible oxidation products of MWCNTs like CO or CO_2 could be detected. In addition, the support function of MWCNTs substrate enables the OER to occur primarily on Co_3O_4 surfaces, which can decrease the corrosion of MWCNT thus improve the stability of the hybrid. As shown in Figure 3a, the current response in LSV of MWCNT almost can be ignored, illustrating the current response from MWCNT corrosion can be excluded in that of Co_3O_4@MWCNT.

4) Electrochemical impedance spectroscopy (EIS) was shown in Figure 4c. The values of Rct can be calculated by fitting of the Nyquist plot. The Rct of Co_3O_4@MWCNT, Co_3O_4-MWCNT and Co_3O_4 are 4.2 Ω, 5.1 Ω, and 6.5 Ω, respectively. Iillustrating Co_3O_4@MWCNT exhibited the smallest charge transfer resistance, indicating that the introduction of MWCNT apparently improved the efficiency of charges to shuttle between electrode and KOH solution. We believe that, with the assistance of DETA, Co_3O_4 nanaorods could be closely attached to MWCNTs, offering a facile electron transport route, as well as facilitating electrochemical reactions at the surface. Such a synergetic effect between Co_3O_4 and MWCNTs was illustrated is Figure 4d. On one hand, the OER was promoted at the anchored Co_3O_4 nanaorods possessing highly activated [110] crystalline surface, on the other hand, the mildly MWCNTs transfer easily the produced electrons to the out circuit during the water oxidation.

4. Conclusion

We have successfully synthesized Co_3O_4 nanorods decorated MWCNTs with the assistance of DETA via a simple strategy. The obtained Co_3O_4@MWCNT sample reveals well-defined structure of 1D nanorods winding around 1D nanotube. In comparison with Co_3O_4-MWCNT, pure Co_3O_4 nanorods and MWCNTs, the Co_3O_4@MWCNT hybrid exhibits prominent catalytic activity towards oxygen evolution reaction (OER) in alkaline electrolytes. Moreover, galvanostatic and chromoamperomatic measurements reveal that Co_3O_4@MWCNT owns promising stability in alkaline solution for long-term test.

HRTEM results demonstrates that the nanorod-shaped Co_3O_4 in the hybrid are composed of highly activated [110] crystalline surface, affording improved OER activity for the Co_3O_4@MWCNT hybrid. Moreover, a synergistic effect between MWCNTs and the ancored Co_3O_4 nanorods may also help to promote the interfacial electron transfer at surfaces and improve the OER performance. This work can not only essentially provide a facile strategy to prepare highly efficient electrocatalyst for OER, but also easily be expanded to prepare other 1D carbon material combined 1D metal oxides nanostructured composite for different applications, such as catalysis, sensors, and energy storage and conversion.

Supporting Information

Linear sweep voltammetry curves (LSVs) of Co_3O_4@MWCNT and Co_3O_4 in 0.1 M KOH, LSVs with and without iR correction, XPS spectrum, Gas chromatograph, a summary of turnover frequency for different catalysts. This material is available free of charge via the Internet.

Corresponding Author

*Ke-Ning Sun: Email: bitkeningsun@163.com.

**Yi-Ming Yan: Email: bityanyiming@163.com.

Notes

The authors declare no competing financial interest.

Author Contributions

The manuscript was written through contributions of all authors. All authors have given approval to the final version of the manuscript.

Acknowledgment

Financial supports from the Ministry of Science and Technology (2012DFR40240), National Natural Science Foundation of China (Grant nos. 21175012), and the Chinese Ministry of Education (Project of New Century Excellent Talents in University) are gratefully acknowledged.

References

1 S. U. M. Khan, M. Al-Shahry and W. B. Ingler, *Science,* 2002, **297**, 2243-2245.

2 M. Gratzel, *Nature,* 2001, **414**, 338-344.

3 J. L. Dempsey, A. J. Esswein, D. R. Manke, J. Rosenthal, J. D. Soper and D. G. Nocera, *Inorg. Chem.,* 2005, **44**, 6879-6892.

4 K. Zeng and D. K. Zhang, *Prog. Energy Combust. Sci.,* 2010, **36**, 307-326.

5 C. C. L. McCrory, S. Jung, J. C. Peters and T. F. Jaramillo, *J. Am. Chem. Soc.,* 2013, **135**, 16977-16987.

6 D. E. Hall, *J. Electrochem. Soc.,* 1983, **130**, 317-321.

7 M. E. Lyons and L. D. Burke, *J. Chem. Soc., Faraday Trans. 1,* 1987, **83**, 299-321.

8 J. Divisek, P. Malinowski, J. Mergel and H. Schmitz, *Int. J. Hydrogen Energy,* 1988, **13**, 141-150.

9 Y. Yamashita, M. Tada, M. Kakihana, M. Osada and K. Yoshida, *J. Mater. Chem.*, 2002, **12**, 1782-1786.

10 F. A. Frame, T. K. Townsend, R. L. Chamousis, E. M. Sabio, T. Dittrich, N. D. Browning and F. E. Osterloh, *J. Am. Chem. Soc.*, 2011, **133**, 7264-7267.

11 *Electrochemical Oxygen Technology*; Kinoshita, K.; Wiley: Interscience, New York, 1992.

12 R. Brimblecombe, A. Koo, G. C. Dismukes, G. F. Swiegers and L. Spiccia, *J. Am. Chem. Soc.*, 2010, **132**, 2892-2894.

13 Q. Liu, J. Jin and J. Zhang, *ACS Appl. Mater. Interfaces*, 2013, **5**, 5002-5008.

14 A. J. Esswein, M. J. McMurdo, P. N. Ross, A. T. Bell and T. D. Tilley, *J. Phys. Chem. C*, 2009, **113**, 15068-15072.

15 Q. Yin, J. M. Tan, C. Besson, Y. V. Geletii, D. G. Musaev, A. E. Kuznetsov, Z. Luo, K. I. Hardcastle and C. L. Hill, *Science*, 2010, **328**, 342-345.

16 D. K. Zhong, M. Cornuz, K. Sivula, M. Grätzel and D. R. Gamelin, *Energy Environ. Sci.*, 2011, **4**, 1759-1764.

17 M. Hamdani, R. Singh and P. Chartier, *Int. J. Electrochem. Sci*, 2010, **5**, 556-577.

18 J. Wu, Y. Xue, X. Yan, W. Yan, Q. Cheng and Y. Xie, *Nano Res.*, 2012, **5**, 521-530.

19 X. Lu and C. Zhao, *J. Mater. Chem. A*, 2013, **1**, 12053-12059.

20 X. Li, Y. Jia, J. Wei, H. Zhu, K. Wang, D. Wu and A. Cao, *ACS Nano*, 2010, **4**, 2142-2148.

21 B. Li, J. Wang, Y. Yuan, H. Ariga, S. Takakusagi and K. Asakura, *ACS Catal.*, 2011, **1**, 1521-1528.

22 Y. Liang, Y. Li, H. Wang and H. Dai, *J. Am. Chem. Soc.*, 2013, **135**, 2013-2036.

23 Y. Liang, H. Wang, P. Diao, W. Chang, G. Hong, Y. Li, M. Gong, L. Xie, J. Zhou and J. Wang, *J. Am. Chem. Soc.*, 2012, **134**, 15849-15857.

24 T. Nakagawa, C. A. Beasley and R. W. Murray, *J. Phys. Chem. C,* 2009, **113**, 12958-12961.

25 X. W. Xie, Y. Li, Z. Q. Liu, M. Haruta and W. J. Shen, *Nature,* 2009, **458**, 746–749.

26 Y. Wang, Z. Zhong, Y. Chen, C. T. Ng and J. Lin, *Nano Res.,* 2011, **4**, 695-704.

27 L. Hu, Q. Peng and Y. Li, *J. Am. Chem. Soc.,* 2008, **130**, 16136-16137.

28 C. Y. Ma, Z. Mu, J. J. Li, Y. G. Jin, J. Cheng, G. Q. Lu, Z. P. Hao and S. Z. Qiao, *J. Am. Chem. Soc.,* 2010, **132**, 2608-2613.

29 J. Yang and T. Sasaki, *Cryst. Growth Des.*, 2010, **10**, 1233-1236.

30 S. Jiang and S. Song, *Appl. Catal. B: Environ.*, 2013, **140**, 1-8.

31 Y. Liang, H. Wang, P. Diao, W. Chang, G. Hong, Y. Li, M. Gong, L. Xie, J. Zhou and J. Wang, *J. Am. Chem. Soc.*, 2012, **134**, 15849-15857.

32 T. H. Yoon and Y. J. Park, *Nanoscale Res. Lett.*, 2012, **7**, 1-4.

33 J. Lang, X. Yan and Q. Xue, *J. Power Sources*, 2011, **196**, 7841-7846.

34 Z. Fang, W. Xu, T. Huang, M. Li, W. Wang, Y. Liu, C. Mao, F. Meng, M. Wang and M. Cheng, *Mater. Res. Bull.,* 2013, **48**, 4419-4423.

35 S. K. Gill, A. M. Shobe and L. J. Hope−Weeks, *Scanning,* 2009, **31**, 132-138.

36 L. Manna, E. C. Scher, L.-S. Li and A. P. Alivisatos, *J. Am. Chem. Soc.,* 2002, **124**, 7136-7145.

37 X. Xie, P. Shang, Z. Liu, Y. Lv, Y. Li and W. Shen, *J. Phys. Chem. C*, 2010, **114**, 2116-2123.

38 G. Zhang, L. Dang, L. Li, R. Wang, H. Fu and K. Shi, *Cryst. Eng. Comm.*, 2013, **15**, 4730-4738.

39 D. Gallant, M. Pezolet and S. Simard, *J. Phys. Chem. B*, 2006, **110**, 6871-6880.

40 V. Hadjiev, M. Iliev and I. Vergilov, *J. Phys. C: Solid State Phys.*, 1988, **21**, L199.

41 W. Wang and G. Zhang, *J. Cryst. Growth*, 2009, **311**, 4275-4280.

42 C. Y. Ma, Z. Mu, J. J. Li, Y. G. Jin, J. Cheng, G. Q. Lu, Z. P. Hao and S. Z. Qiao, *J. Am. Chem. Soc.*, 2010, **132**, 2608-2613.

43 X. Xie, Y. Li, Z.-Q. Liu, M. Haruta and W. Shen, *Nature*, 2009, **458**, 746-749.

Table of Content

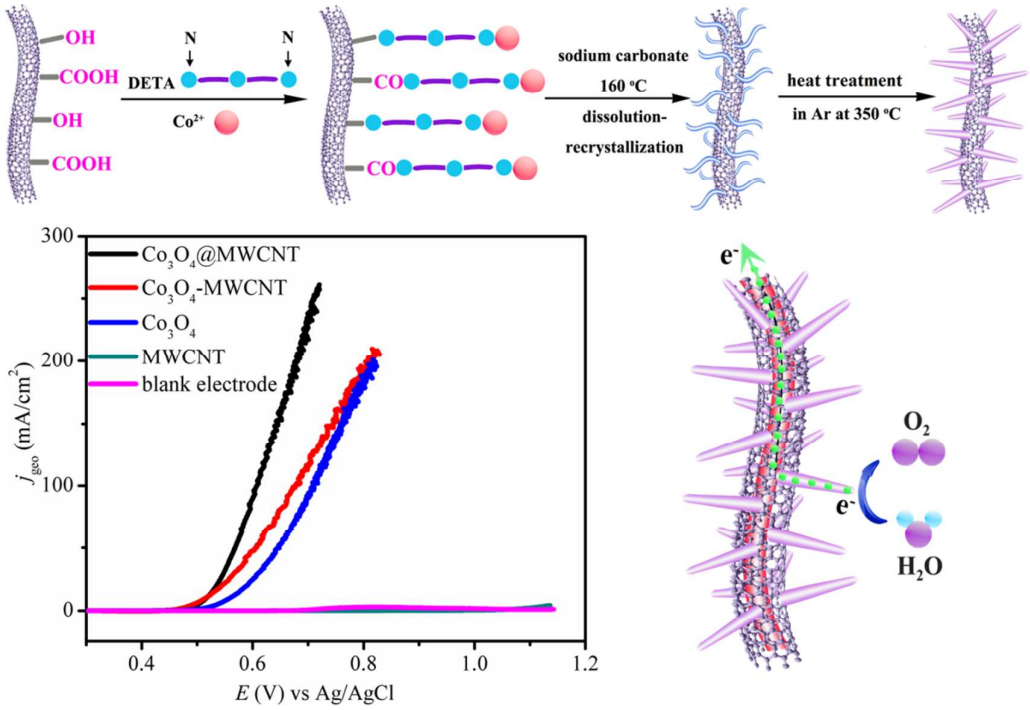

We report the preparation of Co_3O_4@MWCNT with the assistance of DETA and use it as a high performance OER catalyst.